RESEARCH ARTICLE | OCTOBER 10 2024

Scalable ultra-strong light–matter coupling at THz frequencies using graded alloy parabolic quantum wells *⊗*

P. Goulain ⁽¹⁾; M. Jeannin ⁽¹⁾; C. Deimert ⁽¹⁾; T. Blaikie ⁽¹⁾; S. Pirotta; A. Wright; A. De Vetter; M. Mičica; S. Dhillon ⁽¹⁾; Z. R. Wasilewski ⁽¹⁾; R. Colombelli ¹ ⁽¹⁾; J.-M. Manceau ¹ ⁽¹⁾



Appl. Phys. Lett. 125, 153503 (2024) https://doi.org/10.1063/5.0225733





Articles You May Be Interested In

THz intersubband absorption in n-type $Si_{1-x}Ge_x$ parabolic quantum wells

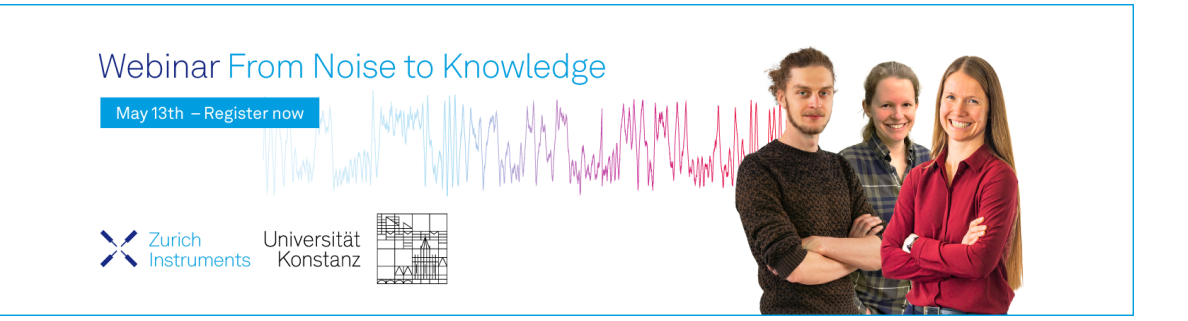
Appl. Phys. Lett. (April 2021)

The thermally coupled imager: A scalable readout architecture for superconducting nanowire single photon detectors

Appl. Phys. Lett. (September 2022)

Scalable fabrication of hemispherical solid immersion lenses in silicon carbide through grayscale hard-mask lithography

Appl. Phys. Lett. (April 2023)





Scalable ultra-strong light-matter coupling at THz frequencies using graded alloy parabolic quantum wells

Cite as: Appl. Phys. Lett. **125**, 153503 (2024); doi: 10.1063/5.0225733 Submitted: 26 June 2024 · Accepted: 30 September 2024 · Published Online: 10 October 2024







P. Goulain, 1 1 M. Jeannin, 1 C. Deimert, 2 T. Blaikie, 2 S. Pirotta, 1 A. Wright, 3 A. De Vetter, 3 M. Mičica, 3 S. Dhillon, 3 D Z. R. Wasilewski, 2,4,5,6 D R. Colombelli, 1,0 D and J.-M. Manceau^{1,0} D

AFFILIATIONS

¹Centre de Nanosciences et de Nanotechnologies, CNRS UMR 9001, Université Paris-Saclay, 91120 Palaiseau, France

ABSTRACT

We demonstrate scalable ultra-strong light–matter coupling with intersubband polaritons in a truly harmonic confining potential. The harmonicity grants immunity from electron–electron interactions, a protection guaranteed by the Kohn theorem, allowing the intersubband transition frequency to be lowered while keeping the light–matter interaction strength constant. In principle, this procedure permits increasing the relative coupling strength ($\eta = \Omega_{\rm Rabi}/\omega_{12}$) at will. We measure a record low intersubband transition at 1.24 THz and a lower polaritonic mode at 920 GHz, below the barrier of 1 THz. The system exhibits a η ratio of 0.24, fully in the ultra-strong coupling regime, and remains stable up to 78 K. This approach is valuable for future non-adiabatic quantum electrodynamic experiments at long wavelengths.

Published under an exclusive license by AIP Publishing. https://doi.org/10.1063/5.0225733

Increasing the strength of the light–matter interaction well beyond the system decoherence rates—the so-called ultra-strong light–matter coupling regime—has been a recent focus of much research in a variety of material systems. ^{1,2} In such a regime, the effects of the counter-rotating terms of the Hamiltonian, usually neglected, become sizable and potentially observable. The promise is to extend quantum effects and technologies into the THz range of the spectrum, ³ with—for instance—the possibility to emit correlated photon pairs when abruptly modulating such a system ^{4–6} or probing quantum phase transition electrically. ⁷

To gauge when a system enters the ultra-strong coupling (USC) regime, a first figure of merit was adopted: the ratio between the Rabi frequency ($\Omega_{\rm Rabi}$) and the resonant frequency of the two-level system (ω_{12}), $\eta = \Omega_{\rm Rabi}/\omega_{12}$. With η greater than 0.1, the system starts to

deviate from the rotating wave approximation: this is generally considered the threshold value for operation in the USC regime. Recently, another parameter has been introduced, $U=\sqrt{\eta\times C}$, where C, named cooperativity, is defined as $C=4\Omega_{\rm Rabi}^2/\kappa\gamma$. κ and γ are the cavity and transition linewidths, respectively. A value of $U\geq 1$ indicates that the system operates in the USC regime with a high degree of coherence, allowing access to its physics. To date, superconducting qubits are the most advanced system even though they do not show the highest values of η .

The first demonstrations of USC regime relied on intersubband transitions (ISBTs) in microcavities. Such a system appeared ideal to reach the USC as the transition can be designed in the THz range, while the Rabi frequency can be large since it is directly proportional to the square root of the activated dopants density (n_{2D}) in the

²Department of Electrical and Computer Engineering, University of Waterloo, 200 University Ave W, Waterloo, Ontario N2L 3G1, Canada

³Laboratoire de Physique de l'Ecole normales supérieure, Université PSL, CNRS, Sorbonne Université, Université Paris Cité, F-75005 Paris, France

⁴Institute for Quantum Computing, University of Waterloo, 200 University Ave W, Waterloo, Ontario N2L 3G1, Canada

⁵Waterloo Institute for Nanotechnology, University of Waterloo, 200 University Ave W, Waterloo, Ontario N2L 3G1, Canada

⁶Department of Physics and Astronomy, University of Waterloo, 200 University Ave W, Waterloo, Ontario N2L 3G1, Canada

^{a)}Authors to whom correspondence should be addressed: raffaele.colombelli@c2n.upsaclay.fr and jean-michel.manceau@c2n.upsaclay.fr

heterostructure.4 In such systems, the Rabi frequency is equal to $\Omega_R = \sqrt{f_w}\omega_p/2$, where f_w is the overlap factor between the intersubband current and the electromagnetic mode, while ω_p is the plasma frequency expressed as $\omega_p = \sqrt{f_{12}e^2n_{2D}/\varepsilon\varepsilon_0m^*L_{QW}}$, where f_{12} is the oscillator strength between the first and second subband, m* is the electron's effective mass in GaAs, and $L_{\rm OW}$ is the length of the period comprising one well and one barrier. In fact, after the first demonstrations of USC using ISBT, 8,9 evidence of deviation from the linear interaction Hamiltonian was obtained with an optimized mode volume at THz frequencies. 10 Then, the doping density was used as the primary tuning knob to further increase the coupling strength leading to the observation of a very large polaritonic gap using multisubband plasmons at Mid-InfraRed (MIR) frequencies. 11,12 Further improvement came with inter-Landau level transitions and sub-wavelength resonators reaching η equal unity 13,14 at subterahertz frequencies. The latter operates only at very low temperatures ($\leq 1.5 \, \mathrm{K}$) and elevated magnetic fields.

In the quest to further increase η , it was understood that ISBTs in square quantum wells suffer strong limitations and that η could not be further improved by lowering the transition frequency. As thoroughly discussed in Ref. 15, for a dopant density sufficient to enter the strong coupling regime, the ISBT would inherently be locked at a lower frequency of ~2.5 THz. Furthermore, due to the collective interaction terms, an ISBT is renormalized in frequency by the depolarization shift as follows: $\tilde{\omega} = \sqrt{\omega_{12}^2 + \omega_p^2}$, where $\omega_{\rm p}$ is the plasma frequency of the two-dimensional gas. In turn, any further increase in the doping would lead to a blueshift of the transition, hence leaving the relative coupling strength η unchanged.

Recently, we have shown that it is possible to overcome this intrinsic limit by employing a semiconductor-based artificial system that is not affected by Coulomb interaction. The core idea is to rely on the properties of the harmonic oscillator, one of the workhorses of quantum mechanics. Parabolic energy potentials made of digitally graded alloys have been previously employed to demonstrate strong light-matter coupling at terahertz (THz) frequencies 16-18 with the promise of room-temperature operation. However, their optical performance was relatively poor, presumably because of interface roughness broadening resulting from the interdigitated epitaxial growth technique. An alternative approach to this problem is to continuously grade the alloy composition during the growth with high accuracy. It necessitates precise modulation of time-varying group-III fluxes, which poses challenges within a conventional molecular beam epitaxy setup due to the thermal lag in the response of the group III cell. Deimert and Wasilewski devised an approach utilizing a transfer function model to harness the effusion cell thermal dynamics, as described in Refs. 19 and 20. This methodology has resulted in high-performance THz ISB

transitions with stable narrow linewidths of 11% of the central frequency up to 150 K (Ref. 21) and, more recently, in ISB polaritons with unprecedented linewidth, operating at the onset of the USC with $\eta=0.12$. Note that a similar graded alloy composition technique has also been applied to the chemical vapor deposition growth of Si_{1-x}Ge_x, seeking the same promise of room-temperature operation. ^{22–24}

In the present article, we build on this recent demonstration to unlock the technique's full potential. We have implemented a series of graded parabolic quantum wells (PQW) with identical Rabi frequency as in Ref. 15, but whose operating frequency is gradually redshifted from 1.74 THz down to 1.26 THz. Inserting the samples in judiciously designed micro-cavities leads to operation in the USC regime, with intersubband polaritons at the record-low frequency of 920 GHz. The results presented here are taken at 10 K, but operation up to 78 K with good performance is shown in the supplementary material. Not only are the results obtained at much higher temperatures than the current technology established with Landau polaritons, but we have reversed the approach: we decrease the frequency instead of increasing the Rabi frequency. Hence, solely by lowering the transition resonant frequency, we show that we can double the light–matter relative coupling strength η from an initial value of 0.12 right up to 0.24.

Using the software NextNano, we have designed three different PQWs with a central frequency below 2 THz (Fig. S1). The parabolic energy potential is faithfully reproduced by a graded variation of the aluminum composition of which the profiles are presented in the supplementary material (Fig. S2), as well as their expected absorption frequency. Particular care was taken in the design to obtain a constant Rabi frequency across all three structures and to be equal to sample G0642 published in Ref. 15 as a matter of comparison. All three structures are detailed in Table I. For all three samples, the Si doping is introduced as δ layers at the barrier center with a nominal sheet density of $5 \times 10^{10} \, \mathrm{cm}^{-2}$, ensuring a similar Rabi frequency as sample G0642. Cladding layers of 50 nm AlGaAs and cap layers of 30 nm GaAs are placed on the top and bottom of the structure. We have also kept the overall heterostructure thickness constant at 1.205 μ m.

To assess the optical performance of the fabricated structures, samples were shaped into a multi-pass prism, with the facets polished at a 45° angle. A titanium/gold metallization was applied to the sample top surface to maximize the electric field overlap with the parabolic quantum well repetitions. Samples were placed within a continuous-flow cryostat housed in a Fourier transform infrared spectrometer that can be placed under vacuum. A polyethylene polarizer was used to select the polarization of the Globar source that was directed onto the sample. The transmitted spectra were measured utilizing a liquid-helium-cooled Si bolometer. Due to the ISBT selection rule, PQWs selectively absorbed transverse magnetic (TM) polarized light. In order to isolate this absorption, ratios were computed between the

TABLE I. Sample parameters.

	Targeted frequency (THz)	Parabola length (nm)	Barrier length (nm)	Doping (cm ⁻²)	Aluminum composition	Number of repetitions
G0958	1.4	189	20	5×10^{10}	From 2% to 20%	5
G0960	1.6	165	44	5×10^{10}	From 2% to 20%	5
G0962	1.9	139	70	5×10^{10}	From 2% to 20%	5

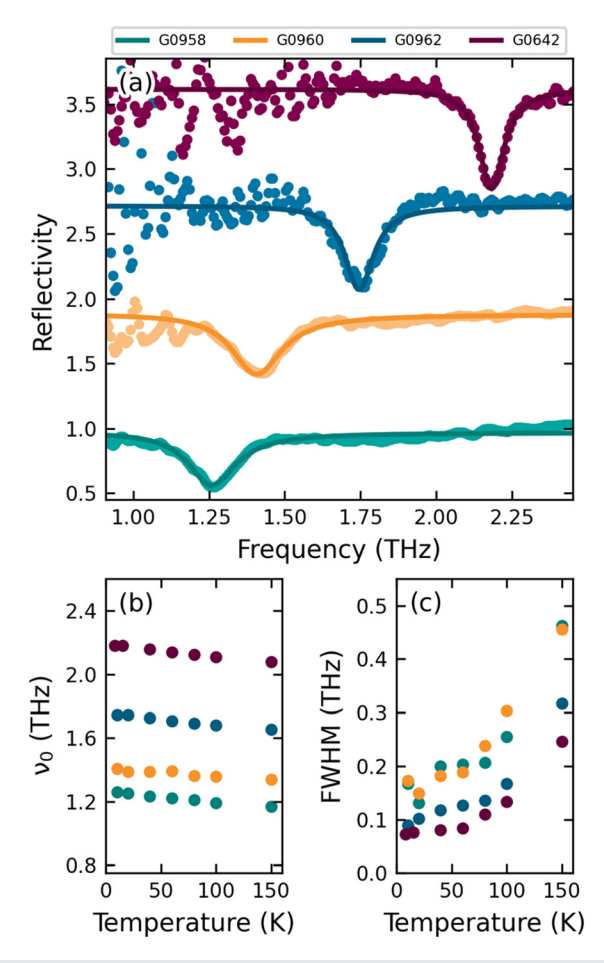


FIG. 1. (a) Transmittance measurement of the samples shaped in the multipass configuration recorded at 10 K. The curves are vertically shifted for clarity. (b) Central frequency of the ISB transition for each measured sample as a function of the temperature. (c) Full width at half maximum (FWHM) as a function of the temperature.

transmission spectra for TE- and TM-polarized incident light. Figure 1 (a) shows the transmittance measurement of the three samples at a temperature of 10 K. By modeling the transition with a diagonal dielectric tensor,²⁵ we can fit the experimental data and extract the transition's central frequency and linewidth to evaluate the structure's performance as a function of the temperature. Note: as a matter of completeness, we directly compared it to sample G0642 from the earlier paper. 13 Note that the results from G0642 were obtained with a different bolometer and that the number of scans is increased as we measure samples with a lower transition, hence significantly reducing the signal to noise ratio at short frequencies. As a first observation, we note that we are slightly off the design by \sim 150 GHz for each sample. We recorded central frequency at 1.74 THz, 1.41 THz and the lowest one at 1.24 THz, which is, to date, the lowest ISB transition measured without the help of a magnetic field. As presented in Figs. 1(b) and 1(c), the central frequency remains relatively stable over the whole temperature range, and the 150 GHz shift could reasonably be attributed to the conduction band offset variation. The linewidth shows

excellent performance at 10 K, although it broadens as we lower the transition energy, from 91 GHz at 1.74 THz central frequency ($\gamma_{12}/\omega_{12}=5\%$) up to 168 GHz for the 1.26 THz ($\gamma_{12}/\omega_{12}=13\%$). Below 78 K, performance remain stable, while above 78 K, we witness the same trend of linewidth degradation for all the samples—the origin of this degradation has not been elucidated yet. While the usual scattering mechanisms, such as ionized impurities and interface roughness, can be excluded, we speculate that the present samples might slightly deviate from a purely parabolic energy potential. Hence, while lowering the transition, electrons populate non-perfectly equidistant levels as they spread on the energy ladder, leading to a gradual degradation of the linewidth. Measurements up to 300 K are shown in the supplementary material.

We then explore the light-matter interaction by embedding these samples in microcavities. These are 1D metal-insulator-metal stripes where light is confined at a subwavelength scale with TM polarization. ²⁶ The details of the fabrication can be found in Ref. 27. The active region thickness being $1.2 \,\mu\text{m}$, the confined TM mode forms a standing-wave pattern with the resonant frequency defined by the metal stripe width. As depicted in the numerical simulation of Fig. 2(a), the photonic mode will disperse as a function of the stripe sizes, ensuring that the classic anti-crossing signature of the strongcoupling regime can be obtained, enabling a precise gauging of the interaction strength. Using the same experimental setup, we first probed the samples closest to the anti-crossing position at an incident angle of 10°. Figure 2(b) shows the reflectance measurement recorded at 10 K, where one can observe a radical departure from the linear reflectance with the apparition of the two new polaritonic modes. Note that we verified that G0958 and G0960 can operate with similar performance up to 78 K (see the supplementary material).

To infer the Rabi frequency and the strength of the light–matter interaction, we measured all the fabricated samples and reconstructed the polaritonic dispersion. Since our bolometer was limited in terms of signal-to-noise ratio at frequencies below 1.2 THz, we employed a THz time-domain spectrometer to record the polariton reflectance. Although we are using a high-resolution photoconductive antenna approach, the spectral resolution remains limited to $\delta \nu = 50\,\mathrm{GHz}$ because the quartz windows on the cryostat induce echoes on the time trace. Figure 3 presents the dispersion for each stripe size and each sample. The points are the experimental minima of the reflectance, while the solid line is a fit using the roots of the polaritonic secular expressed as

$$(\omega - \omega_c^2)(\omega - \tilde{\omega}_{12}^2) = f_w \omega_P^2 \omega_c^2,$$

where $\omega_{\rm c}$ is the cavity resonance numerically calculated, $\tilde{\omega}_{12}$ is the measured transition, while $f_{\rm w}$ is the overlap factor between the ISB current and the electromagnetic mode, considering that the EM mode is strictly confined below the metallic stripe. The experimental reflectance curves are presented in the supplementary material, while the dispersion of sample G0642 can be found in Ref. 15. On Figs. 3(a)–3(c), the polaritonic gap, represented with the asymptotes (dotted lines), opens as the transition frequency redshifts, demonstrating a clear signature of the ultra-strong light–matter interaction. Interestingly, on the lowest frequency transition, we observe a lower polaritonic branch pointing at 920 GHz, below the 1 THz threshold of polaritons based on ISB transitions.

The Rabi frequency for each sample can be extracted from the dispersion curve. The sole fitting parameter used with the secular

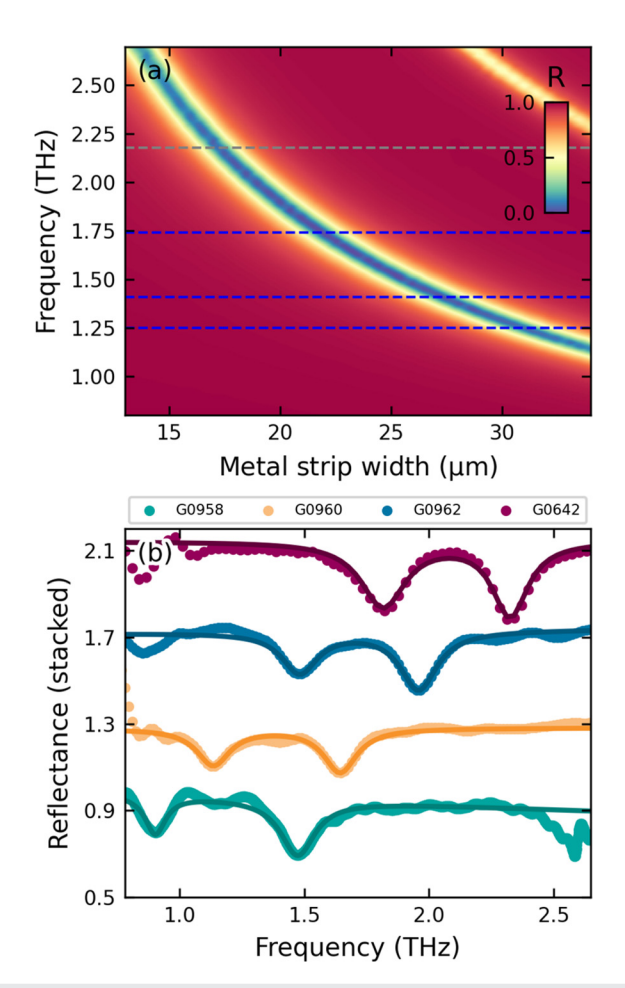


FIG. 2. (a) Numerical simulation of the photolithographic dispersion. The color plot presents the reflectivity of an empty cavity as a function of the metal strip width. The fundamental mode follows the equation $f_{\rm TM00}=c/2ns$, where s is the metallic stripe size. The position of the ISB transitions of all the samples is depicted in dashed lines. (b) Experimental reflectance spectra of all the samples recorded at 10 K. The curves are vertically shifted for clarity. The lines are the fit obtained from the numerical simulations.

equation is the Rabi frequency. Figure 3(d) shows the extracted values of the Rabi splittings, which are stable, consistently with the design, at around 0.49 THz. This corresponds to a calculated sheet carrier density in the range of $5 \times 10^{10} \, \text{cm}^{-2}$, in excellent agreement with the nominal value. Note that doping layers were introduced in the cap layers $(n_{3d} = 3.3 \times 10^{18} \, \text{cm}^{-3})$, helping to minimize the depletion due to Fermi-level pinning in the proximity of the metal layers. We can then compute the relative coupling strength from the extracted Rabi splitting. Figure 3(e) clearly reveals that, by solely lowering the transition frequency, we have doubled the relative coupling strength of the lightmatter interaction from $\eta = 0.12$ up to a value of 0.24 for the lowest energy transition. Even though η has doubled, the linewidth degradation hampers a clear improvement of the cooperativity parameter and the estimated U remains about 1.7 as in Ref. 15. Although relatively low in comparison with what can be achieved with superconducting circuits, our system based on PQWs is promising for several reasons.

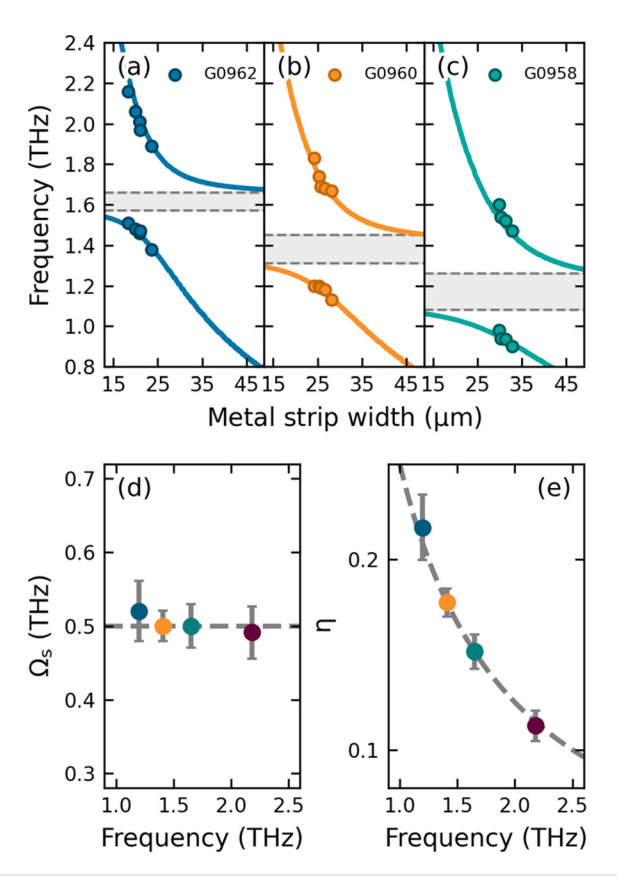


FIG. 3. (a)–(c) Polaritonic reflectance minima recorded with time domain spectroscopy (dots). The lines are a fit using the secular polaritonic equation. The dashed lines are the asymptotes revealing the opening of the polaritonic gap. (d) Extracted Rabi frequency from the dispersion plots as a function of ISB transition frequency. (e) Calculated coupling strength for the three samples, along with sample G0642 (highest frequency point).

In the present manuscript, no particular efforts were devoted to the optimization of the linewidth of the transition. We anticipate that if we keep the linewidth below 100 GHz while increasing the doping significantly up to a factor 5, we could reach values of U=10, where the quantum electro-dynamic effect can be investigated. Furthermore, such a system is compatible with subwavelength microcavities whose optical density of states can be modulated on ultra-fast timescales, which is the prerequisite for non-adiabatic electrodynamic experiments. Finally, the frequency is ideally centered on the bandwidth of the electro-optic and quantum capacitance detectors, which have been, respectively, used to probe quantum vacuum fluctuations, 31,32 or single photon at 1.5 THz. 33,34

In conclusion, we have demonstrated that parabolic energy potentials permit circumventing inherent limitations imposed by Coulomb interaction. The harmonic oscillator allows lowering the ISBT energy down to 1.24 THz, a range which was so far unreachable. Once coupled to a resonant electromagnetic mode, we demonstrated the operation in the USC regime and the possibility of scaling the strength of the interaction solely by lowering the transition frequency. This semiconductor platform and approach offer interesting

perspectives for extending non-adiabatic quantum electrodynamic experiments to long wavelengths. We also anticipate that the advantage of the reduced interface roughness scattering could be beneficial to experiments exploring bosonic final state stimulation.³⁵

See the supplementary material for the numerical Poisson–Schrödinger simulation that has been done to design the parabolic quantum well measured experimentally; the full set of ISB transition transmittance measurements as a function of the temperature as well as the reflectance measurement of the polaritonic sample at the anticrossing as a function of the temperature; and finally, the reflectance of the samples measured to reconstruct the polaritonic dispersion.

The authors thank N. Zerounian for lending the Sibolometer. This work was partially supported by the European Union through FET-Open Grant MIRBOSE (No. 737017). It was done within the C2N micro nanotechnologies platforms and partly supported by the RENATECH network and the General Council of Essonne. We thank the C2N cleanroom staff for their technical help.

AUTHOR DECLARATIONS Conflict of Interest

The authors have no conflicts to disclose.

Author Contributions

P. Goulain: Conceptualization (equal); Formal analysis (equal); Investigation (equal); Writing – review & editing (equal). M. Jeannin: Data curation (equal); Investigation (equal); Writing - review & editing (equal). C. Deimert: Conceptualization (equal); Formal analysis (equal); Investigation (equal); Writing - review & editing (equal). T. Blaikie: Investigation (equal). S. Pirotta: Investigation (equal); Writing - review & editing (equal). A. Wright: Investigation (equal). A. De Vetter: Investigation (equal). M. Mičica: Investigation (equal). S. Dhillon: Funding acquisition (equal); Supervision (equal); Writing - review & editing (equal). Z. R. Wasilewski: Funding acquisition (equal); Supervision (equal); Writing - review & editing (equal). R. Colombelli: Conceptualization (equal); Formal analysis (equal); Funding acquisition (equal); Writing - original draft (equal). J.-M. Manceau: Conceptualization (equal); Data curation (equal); Formal analysis (equal); Funding acquisition (equal); Investigation (equal); Supervision (equal); Writing – original draft (equal).

DATA AVAILABILITY

The data that support the findings of this study are available from the corresponding authors upon reasonable request.

REFERENCES

- ¹A. Frisk Kockum, A. Miranowicz, S. De Liberato, S. Savasta, and F. Nori, "Ultrastrong coupling between light and matter," Nat. Rev. Phys. 1(1), 19–40 (2019).
- ²P. Forn-Díaz, L. Lamata, E. Rico, J. Kono, and E. Solano, "Ultrastrong coupling regimes of light-matter interaction," Rev. Mod. Phys. **91**(2), 025005 (2019).
- ³Y. Todorov, S. Dhillon, and J. Mangeney, "THz quantum gap: Exploring potential approaches for generating and detecting non-classical states of THz light," Nanophotonics 13(10), 1681–1691 (2024).

- ⁴C. Ciuti, G. Bastard, and I. Carusotto, "Quantum vacuum properties of the intersubband cavity polariton field," Phys. Rev. B **72**(11), 115303 (2005).
- ⁵S. D. Liberato, C. Ciuti, and I. Carusotto, "Quantum vacuum radiation spectra from a semiconductor microcavity with a time-modulated vacuum Rabi frequency," Phys. Rev. Lett. 98(10), 103602 (2007).
- ⁶C. M. Wilson, G. Johansson, A. Pourkabirian, M. Simoen, J. R. Johansson, T. Duty, F. Nori, and P. Delsing, "Observation of the dynamical Casimir effect in a superconducting circuit," Nature 479(7373), 376–379 (2011).
- ⁷U. Iqbal, Y. Todorov, and C. Mora, "Dynamical Coulomb blockade: An all electrical probe of the ultrastrong light-matter coupling regime," Phys. Rev. Res. 6(3), 033097 (2024).
- ⁸E. Dupont, J. A. Gupta, and H. C. Liu, "Giant vacuum-field Rabi splitting of intersubband transitions in multiple quantum wells," Phys. Rev. B 75(20), 205325 (2007).
- ⁹A. A. Anappara, S. De Liberato, A. Tredicucci, C. Ciuti, G. Biasiol, L. Sorba, and F. Beltram, "Signatures of the ultrastrong light-matter coupling regime," Phys. Rev. B 79(20), 201303 (2009).
- ¹⁰ Y. Todorov, A. M. Andrews, R. Colombelli, S. De Liberato, C. Ciuti, P. Klang, G. Strasser, and C. Sirtori, "Ultrastrong light-matter coupling regime with polariton dots," Phys. Rev. Lett. 105(19), 196402 (2010).
- ¹¹A. Delteil, A. Vasanelli, Y. Todorov, C. Feuillet Palma, M. Renaudat St-Jean, G. Beaudoin, I. Sagnes, and C. Sirtori, "Charge-induced coherence between intersubband plasmons in a quantum structure," Phys. Rev. Lett. 109(24), 246808 (2012).
- ¹²B. Askenazi, A. Vasanelli, A. Delteil, Y. Todorov, L. C. Andreani, G. Beaudoin, I. Sagnes, and C. Sirtori, "Ultra-strong light-matter coupling for designer Reststrahlen band," New J. Phys. 16(4), 043029 (2014).
- ¹³G. Scalari, C. Maissen, D. Turcinkova, D. Hagenmuller, S. De Liberato, C. Ciuti, C. Reichl, D. Schuh, W. Wegscheider, M. Beck, and J. Faist, "Ultrastrong coupling of the cyclotron transition of a 2D electron gas to a THz metamaterial," Science 335(6074), 1323–1326 (2012).
- ¹⁴ A. Bayer, M. Pozimski, S. Schambeck, D. Schuh, R. Huber, D. Bougeard, and C. Lange, "Terahertz light–matter interaction beyond unity coupling strength," Nano Lett. 17(10), 6340–6344 (2017).
- ¹⁵P. Goulain, C. Deimert, M. Jeannin, S. Pirotta, W. J. Pasek, Z. Wasilewski, R. Colombelli, and J.-M. Manceau, "THz ultra-strong light-matter coupling up to 200 K with continuously-graded parabolic quantum wells," Adv. Opt. Mater. 11(9), 2202724 (2023).
- 16 M. Geiser, F. Castellano, G. Scalari, M. Beck, L. Nevou, and J. Faist, "Ultrastrong coupling regime and plasmon polaritons in parabolic semiconductor quantum wells," Phys. Rev. Lett. 108(10), 106402 (2012).
- ¹⁷D. Dietze, A. Benz, G. Strasser, K. Unterrainer, and J. Darmo, "Terahertz metaatoms coupled to a quantum well intersubband transition," Opt. Express 19(14), 13700 (2011).
- ¹⁸B. Paulillo, J.-M. Manceau, L. H. Li, A. G. Davies, E. H. Linfield, and R. Colombelli, "Room temperature strong light-matter coupling in three dimensional terahertz meta-atoms," Appl. Phys. Lett. 108(10), 101101 (2016).
- 19 C. Deimert and Z. R. Wasilewski, "MBE growth of continuously-graded parabolic quantum well arrays in AlGaAs," J. Cryst. Growth 514, 103–108 (2019).
- ²⁰C. Deimert and Z. R. Wasilewski, "Precise control of time-varying effusion cell flux in molecular beam epitaxy," J. Vac. Sci. Technol., A 39(4), 043407 (2021).
- ²¹C. Deimert, P. Goulain, J.-M. Manceau, W. Pasek, T. Yoon, A. Bousseksou, N. Y. Kim, R. Colombelli, and Z. R. Wasilewski, "Realization of harmonic oscillator arrays with graded semiconductor quantum wells," Phys. Rev. Lett. 125(9), 097403 (2020).
- ²²A. Ballabio, J. Frigerio, S. Firoozabadi, D. Chrastina, A. Beyer, K. Volz, and G. Isella, "Ge/SiGe parabolic quantum wells," J. Phys. D 52(41), 415105 (2019).
- ²³M. Montanari, C. Ciano, L. Persichetti, C. Corley, L. Baldassarre, M. Ortolani, L. Di Gaspare, G. Capellini, D. Stark, G. Scalari, M. Virgilio, and M. De Seta, "THz intersubband absorption in n-type Si_{1-x}Ge_x parabolic quantum wells," Appl. Phys. Lett. 118(16), 163106 (2021).
- ²⁴F. Berkmann, T. Venanzi, L. Baldassarre, E. Campagna, E. Talamas-Simola, L. D. Gaspare, C. Corley-Wiciak, G. Nicotra, G. Sfuncia, A. Notargiacomo, E. Giovine, S. Cibella, M. Virgilio, G. Scalari, M. De, and M. Ortolani, "Ultrastrong coupling of Si_{1-x}Ge_x parabolic quantum wells to terahertz microcavities," ACS Photonics 11, 2776–2786 (2024).

- 25 M. Załużny and C. Nalewajko, "Coupling of infrared radiation to intersubband transitions in multiple quantum wells: The effective-medium approach," Phys. Rev. B 59(20), 13043–13053 (1999).
- ²⁶Y. Todorov, L. Tosetto, J. Teissier, A. M. Andrews, P. Klang, R. Colombelli, I. Sagnes, G. Strasser, and C. Sirtori, "Optical properties of metal-dielectric-metal microcavities in the THz frequency range," Opt. Express 18(13), 13886 (2010).
- ²⁷J.-M. Manceau, S. Zanotto, I. Sagnes, G. Beaudoin, and R. Colombelli, "Optical critical coupling into highly confining metal-insulator-metal resonators," Appl. Phys. Lett. **103**(9), 091110 (2013).
- 28K. Maussang, J. Palomo, J.-M. Manceau, R. Colombelli, I. Sagnes, L. H. Li, E. H. Linfield, A. G. Davies, J. Mangeney, J. Tignon, and S. S. Dhillon, "Monolithic echo-less photoconductive switches as a high-resolution detector for terahertz time-domain spectroscopy," Appl. Phys. Lett. 110(14), 141102 (2017).
- ²⁹P. Goulain, A. D. Koulouklidis, J.-M. Manceau, C. Daskalaki, B. Paulillo, K. Maussang, S. Dhillon, J. R. Freeman, L. Li, E. H. Linfield, S. Tzortzakis, and R. Colombelli, "Femtosecond broadband frequency switch of terahertz three-dimensional meta-atoms," ACS Photonics 8, 1097 (2021).

- ³⁰M. Halbhuber, J. Mornhinweg, V. Zeller, C. Ciuti, D. Bougeard, R. Huber, and C. Lange, "Non-adiabatic stripping of a cavity field from electrons in the deepstrong coupling regime," Nat. Photonics 14(11), 675–679 (2020).
- ³¹C. Riek, D. V. Seletskiy, A. S. Moskalenko, J. F. Schmidt, P. Krauspe, S. Eckart, S. Eggert, G. Burkard, and A. Leitenstorfer, "Direct sampling of electric-field vacuum fluctuations," Science 350(6259), 420–423 (2015).
- ³²I.-C. Benea-Chelmus, F. F. Settembrini, G. Scalari, and J. Faist, "Electric field correlation measurements on the electromagnetic vacuum state," Nature 568(7751), 202–206 (2019).
- 33S. Komiyama, O. Astafiev, V. Antonov, T. Kutsuwa, and H. Hirai, "A single-photon detector in the far-infrared range," Nature 403(6768), 405–407 (2000).
- 34P. M. Echternach, B. J. Pepper, T. Reck, and C. M. Bradford, "Single photon detection of 1.5 THz radiation with the quantum capacitance detector," Nat. Astron. 2(1), 90–97 (2017).
- 35M. Knorr, J. M. Manceau, J. Mornhinweg, J. Nespolo, G. Biasiol, N.-L. Tran, M. Malerba, P. Goulain, X. Lafosse, M. Jeannin, M. Stefinger, I. Carusotto, C. Lange, R. Colombelli, and R. Huber, "Intersubband polariton-polariton scattering in a dispersive microcavity," Phys. Rev. Lett. 128(24), 247401 (2022).